Monte Carlo light transport-based blood vessel quantification using linear array photoacoustic tomography

Xiangwei Lin (蔺祥伟), Mingjian Sun (孙明健)*, Naizhang Feng (冯乃章),
Depeng Hu (胡德鹏), and Yi Shen (沈 毅)

Department of Control Science and Engineering, Harbin Institute of Technology, Harbin 150001, China
*Corresponding author: sunmingjian@hit.edu.cn

Photoacoustic tomography is a noninvasive and nonionized biomedical imaging modality but it cannot reveal the inner structure and sideward boundary information of blood vessels in the linear array detection mode. In contrast, Monte Carlo (MC) light transport could provide the optical fluence distribution around the entire vascular area. This research explores the combination of linear array transducer-based photoacoustic tomography and MC light transport in the blood vessel quantification. Simulation, phantom, and *in vivo* experiments are in good correlation with the ultrasound imaging, validating this approach can clearly visualize the internal region of blood vessels from background tissue.

OCIS codes: 170.5120, 100.3020, 110.5120, 170.0110.
doi: 10.3788/COL201715.111701.

Many diseases such as arteriosclerosis, plaque, and angiogenesis around tumors have significant effects on blood vessel formation so that noninvasive imaging and monitoring of blood vessels or vascular lesion-related tissue structure would be a key factor to assess the physiological and pathological status and it has widely attracted the attention of researchers in recent years[1–3]. One of the possible biomedical imaging modalities to quantitatively measure the various vasculature properties is photoacoustic tomography (PAT), which has been utilized in a variety of biological and clinical applications[4–6]. It is a noninvasive imaging modality due to the instant thermo-elastic expansion of either endogenous or exogenous optical contrast agents in biological tissue.

Based on the optical absorption of inherent hemoglobin chromophore inside the blood[7,8], PAT could provide the anatomy and functional imaging in blood vessels non-invasively and nonionized compared with the traditional X-ray angiography[9–12]. The linear array transducer-based PAT assumes the photoacoustic (PA) sources lie in the same plane as thetransducer, resulting a 2D acquisition geometry[13–15]. Therefore, it can be easily integrated with B-mode ultrasound (US) imaging and could precisely realize the architectural analysis such as the location, shape, sizes, axial, and lateral diameter of the vessels. These properties could be further extracted through blood vessel quantification methods based on PA imaging[16,17]. Another advantage of PAT is that it could achieve functional imaging due to the multispectral characteristic of the hemoglobin.

The linear array transducer-based cross-sectional PAT is most widely applied in current research due to its accelerated data acquisition speed, handheld bedside availability, and shared hardware acquisition and software reconstruction with B-scan US in nature. However, the inner blood vessel structure cannot be revealed due to the internal thermal elasticity counteracting each other[18] and the boundary information would be lost because of the limited view problem[19]. Thus, the inside vascular structure and lateral margin could not be completely revealed in this configuration. However, the clinical diagnostics needed to use PA imaging to reveal these structures are desperately required, especially in the evaluation of internal vascular injury-related diseases or hemodynamic measurement inside the vessels.

To solve the challenge of internal vascular imaging, the fluence compensation is applied here based on the PA principle. The initial PA pressure p_0 of the absorber at position r could be calculated by $p_0 = \Gamma\mu_a(r)\Phi(r)$, where Γ is the Gruneisen coefficient, $\mu_a(r)$ is the absorption map, and $\Phi(r)$ is the optical fluence. After compensating the optical fluence Φ, the optical absorption μ_a, which mainly corresponds to the internal vascular geometry, would be approximately recovered[20]. Monte Carlo (MC) light transport is a stochastic and statistical model to depict the local rules of photon propagation in biological tissue[21–23]. Thus, it could provide both the distribution of the optical fluence and the deposited optical energy density by properly assigning the optical absorption and scattering coefficient of the specific tissue constituent[24,25]. This method has been successfully applied in photoacoustically determining the optical absorption coefficient of biological tissue[26–28].

Since the imaging contrast in PAT came from internal optical absorbers, this modality could avoid the injection of any exogenous contrast agent and thus the MC model, which reflects the tissue structure, could be built more accurately. Herein, to resolve the limitations of linear

array transducer-based PAT, our research focuses on combining conventional reflection-mode PAT with MC fluence compensation to determine the inside structure and edge of blood vessels in biological tissue. A series of simulation tests, phantom, and *in vivo* experiments are conducted to validate the feasibility of the proposed approach.

The MC simulation configuration of a numerical artificial vessel phantom to mimic the longitudinal and tangential view of blood vessel geometries is shown in Figs. 1(a) ($z–x$ slice, $y = 0$) and 1(d) ($z–y$ slice, $x = 0$). This phantom (1.00 mm in tangential diameter and 20.00 mm in longitudinal length) is inserted into the 3D cubic background region (20 mm × 20 mm × 20 mm). The optical properties of the background media are the absorption coefficient of $\mu_a = 0.02$ cm^{-1} and the reduced scattering coefficient of $\mu'_s = 15.90$ cm^{-1}, whereas numerical parameters of the artificial vessel are $\mu_a = 3.98$ cm^{-1} and $\mu'_s = 6.70$ cm^{-1}. A uniform distributed laser beam with a diameter of 0.50 cm is utilized to illuminate the center imaging domain. The corresponding laser wavelength is 750 nm and the running time duration of the simulation was 1.0 min.

The optical fluence map at both the longitudinal and tangential directions of the vessel phantom are presented in Figs. 1(b) and 1(e), respectively. The fluence located inside the target tends to be infinitesimal due to the optical absorption and photon scattering. After multiplying the absorption coefficient, Figs. 1(c) and 1(f) are the corresponding optical energy depositions. These deposition maps reveal the fact that the thermoelastic expansion of the absorbers only exists at the vessel boundary, while the internal optical energy deposition is prone to not be strong enough to generate the acoustic waves. This finding gives the guidance on searching the spatial orientations of the PA signal generation if the inside absorbers were distributed uniformly.

The deposited optical energy distribution gained from the above MC light transport model could serve as PA

sources in modeling the initial PA pressure. The K-wave toolbox is chosen here for the fast simulation of the forward PA wave propagation and detection. A linear array US transducer is separately set orthogonally to these two directions of the vessel phantom, and the numerical simulation model can be seen in Figs. 2(a) and 2(b). This linear array transducer has 64 directional elements, with a pitch of 0.30 mm and a center frequency of 7.5 MHz. The pitch size and center frequency are maintained the same with the parameters of the transducer used in the following experiment. The simulation was performed in a cross-sectional plane with a field of view 6.00 mm × 3.50 mm and a pixel size of 0.05 mm × 0.05 mm, as indicated by the blue dashed square in the figure.

The PA images reconstructed by the universal backprojection (BP) method are illustrated in Figs. 3(a) and 3(c), respectively. From these two images, it can be observed that only the vascular edges just below the transducer can be recovered, without any inside or sideward structure information. The reason that this happens is that the generated PA signals can only be detected at two opposite orientations other than the omni direction due to the counteraction of internal thermal elasticity and the limited-view deficiency of the finite aperture.
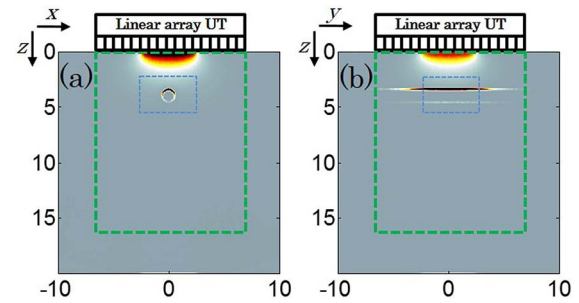
Fig. 2. (Color online) Numerical simulation configurations (a) $x–z$ and (b) $y–z$ direction of the PA wave propagation and detection.
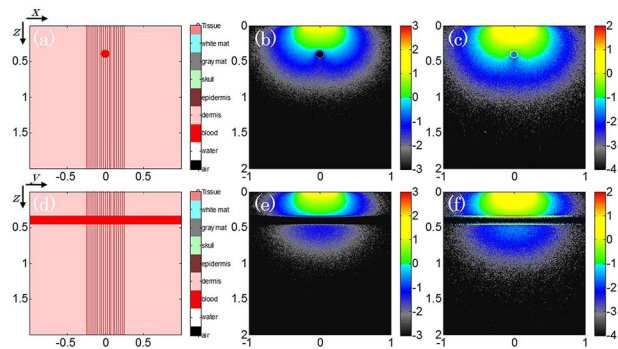
Fig. 1. (Color online) MC light transport model for an artificial blood vessel. The target location and beam pattern are at the (a) longitudinal and (d) tangential direction. The corresponding fluence distribution and the absorbed energy density are (b, c) along the $x–z$ slice ($y = 0$ cm) and (e, f) at the $y–z$ slice ($x = 0$ cm).
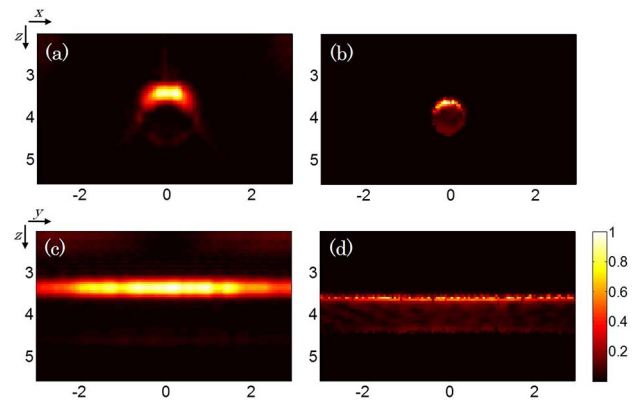
Fig. 3. (Color online) Conventional BP reconstructed PA images (a) and (c), and conventional BP reconstructed PA images (b) and (d) with the fluence compensation from the MC light transport model.

The corresponding depth-resolved raw data from the center channel also validate this hypothesis. There is not a bit of meaningful PA signal locating on the time of arrival of the internal region, resulting in the structure loss in the vessel phantom.

After coupling the laser irradiation pattern obtained in the MC light transport, i.e., Figs. 1(b) and 1(e), the recovered PA images are separately shown in Figs. 3(b) and 3(d). The structure information from the inside and sideward part of the vascular edges can be unfolded clearly in a way that the full structure can be visualized with the optical fluence compensation. These simulation findings verify the hypothesis that the optical contrasts relative to the background media can be imaged in terms of the location, size, and overall geometry of the vessel phantom. The recovered phantom diameter is around 1.00 mm, while the image boundary in the BP reconstruction is somewhat swollen to 1.60 mm. This vessel diameter, extracted from the conventional BP reconstructed PA image, deviates greatly compared with the actual size of the numerical vessel. In addition, the artifacts from the background of the PA image could be reduced, which validates the PA principle that the approximate absorption value could be obtained through the fluence compensation.

For carrying out preclinical studies, a cross-sectional PA imaging system (Fig. 4) has been developed to demonstrate the proposed approach, which consists of optical illumination, acoustic signal acquisition, and data off-line process modules. The optical unit contains a Q-switched Nd:YAG laser (Vibrant 355 II HE, Opotek, USA), emitting a 5 ns width pulse in the tunable near-infrared range. The pulse repetition rate is 10 Hz and the output laser wavelength is 750 nm. The light is delivered through the custom-made optical fiber bundle to ensure the uniform light illumination to the target. The maximum laser fluence at the sample surface is limited to 15 mJ/cm^2, and this value is within the ANSI safety standard.

A linear array transducer adapted to an open research platform (Prodigy, S-Sharp, China) for both PA and US imaging contains 128 elements to acquire the US/PA signal. The external trigger from the laser system is sent to synthesize the receive-only mode on the US array platform. The focal length at the elevational plane of the
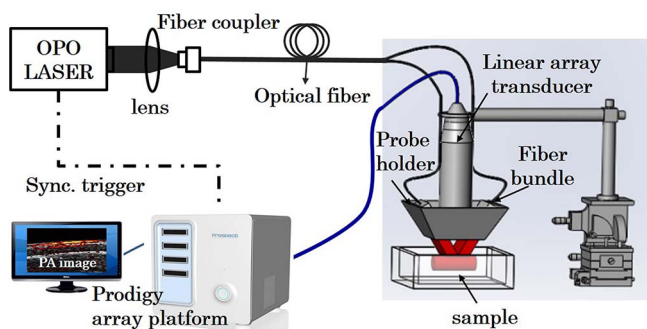
transducer is 20.00 mm and the horizontal aperture is 40.00 mm. The pitch of the transducer is 0.30 mm and each transducer element has a 7.5 MHz center frequency with a fractional bandwidth of 75%. The previous optical fiber bundles are attached to both sides of the transducer and all these objects are integrated into a custom-made housing holder, thus a handheld PA probe would be designed for the experiment.

The raw channel data can be acquired subsequently for off-line postprocessing. The PA images are separately reconstructed by the conventional BP method and BP after the compensation of optical fluence from MC light transport. Additionally, the recovered PA images should be co-registered with the corresponding US images, thus the blood vessel properties can be obtained more completely by evaluating the images from this dual-modality imaging system. As a sequence, the phantom and *in vivo* experiments were conducted. All animal and human experiments described here were carried out in compliance with Harbin Institute of Technology approved protocols.

The aim of the phantom study is to test the feasibility of the imaging system in the tracing and quantification of artificial blood vessels and the related results are shown in Fig. 5. A poleyethylene tube (inner diameter: 2.00 mm) filled with blood from a sacrificed BALB/c nude mouse was designed as the imaging target, as shown in Fig. 5(a). This tube was embedded in the tissue-mimicking phantom (comprised of 4% agar) at about 20.00 mm depth from the surface of the transducer. The light was distributed uniformly around the phantom and PA signals were collected by the above the linear array transducer.

Figures 5(c) and 5(f) are the co-registered US and PA images, which were obtained from the lateral and axis directions, as labelled in Fig. 5(a). Besides the precise location of the blood vessel, the upper boundary and lower boundary could be distinguished easily, while the inside information is lost in the conventional BP method. After integrating the optical fluence map obtained from the MC light transport, i.e., Figs. 5(b) and 5(e), the inside and sideward structure could be visualized. The boundary

Fig. 4. PAT setup based on the linear array transducer.
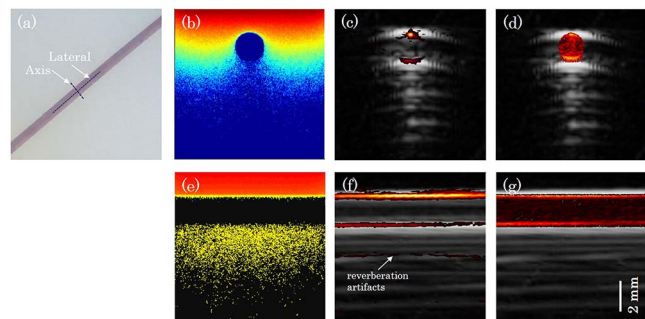
Fig. 5. (Color online) Phantom study of an artificial blood vessel. (a) The photograph of the phantom. (b) The fluence map at the axis view. (c) and (d) are the co-registered US and PA images separately recovered from the BP and the fluence-compensated BP method. (e)–(g) are the results in the same order at the lateral view.

inconsistency could also be eliminated through this fluence compensation if the MC model matches well with the target structure. In virtue of the fluence map, the artificial vessels could be visualized with good resolution and vascular connectivity.

The measured diameter is around 2.00 mm in Figs. 5(d) and 5(g), but it changes to 2.20 mm in Figs. 5(c) and 5(f). The error in quantitative analysis of the vessel diameter is approximately 10%. Here, the location and size of this blood vessel phantom are acquired precisely via the proposed method, especially the tangential and longitudinal diameters. The above results also prove that the main contribution to the laser-induced pressure transient is caused by blood inside the vessel and the vessel wall gives only a minor contribution, which is consistent with Ref. [26]. Additionally, the reverberation artifacts [as indicated by the arrow in Fig. 5(f)] in the PA image could be removed. The artifacts from this blood vessel phantom appear due to reverberation within the tube, which is caused by relatively high light fluence in PA imaging.

Both in the phantom study and in the following *in vivo* experiment, the optical parameters in the MC light transport model, such as absorption, scattering, anisotropy, and refractive index, were assigned as the optical properties of the blood and background tissue at the specific laser wavelength. The geometric structure in the related MC model depended for the most part on the composition of the skin, including epidermis, dermis, and subcutaneous large vessels. The dermis thickness and vascular dimensions were obtained and verified by the B-mode US image measurement. For the *in vivo* experiment, a hierarchy of parallel biological tissue was determined to establish the Monte Carlo model, with an acceptable mismatch between the MC light-transport model and complex tissue structures.

To demonstrate the ability of this dual-modality imaging system to locate and quantitatively measure the properties of human vasculature, the US and PA images acquired from the forearm of one of the authors are presented in Fig. 6. The tests at two different directions, indicated by the arrows in Fig. 6(a), are separately conducted. The reason for choosing these two directions is that the geometry of the blood vessel could be completely evaluated at a full spatial range, which could provide a very powerful imaging tool for clinicians to evaluate vascular-related lesions. The image acquisition time in the *in vivo* experiment was less than 10 s.

Figures 6(b)–6(d) show the cross-sectional images from the axis view. The PA images are displayed within 20 mm × 15 mm, where this field of view exactly matched the US images. The co-registered US/PA images provide the vascular location, the depth or the thickness, and boundary structure information of the blood vessel. The vessel edges, except the parts that are just opposite the linear array transducer, cannot be observed in the PA images. However, the vascular structure could be revealed more completely in Fig. 6(d) after the compensation of the optical fluence. As described beforehand, the field of
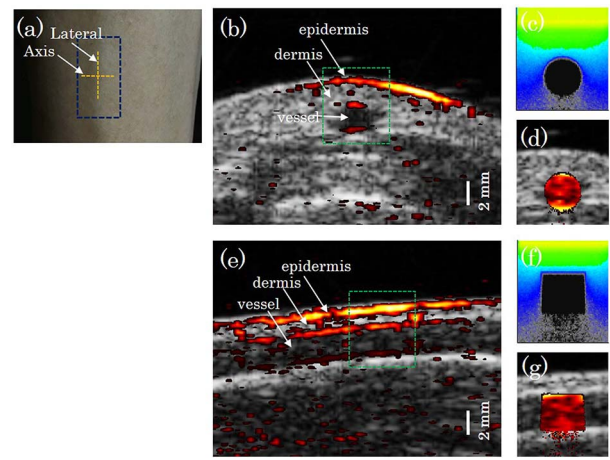
Fig. 6. (Color online) *In vivo* study of a human forearm vessel. (a) The photograph of the vessel. (b) and (d) are the co-registered US and PA images separately recovered from the BP and the fluence-compensated BP method. (c) The fluence map at the axis view. (e)–(g) are the results in the same order at the lateral view.

view in the MC simulation was reduced to parallel multi-layered biological tissue and the positions, boundaries, and shapes of the blood vessels in the MC model are determined by the co-registered US images. Here, the green dashed square in Fig. 6(b) is the region of interest (ROI) and the corresponding fluence map is shown in Fig. 6(c).

After rotating the linear array transducer in the lateral direction, the vascular structure in a broader view could also be detected by the combined cross-sectional US/PA system, as described in Figs. 6(e)–6(g). The internal ROI of the bow-shaped blood vessel is still missing in the conventional BP reconstructed PA images. Through the optical fluence compensation, the vessel profile was clearly visualized from the reconstructed PA images at the depth of around 1.00 mm from the tissue surface. It is of great significance in observing whether the degenerative material accumulates in the inner layer of vascular wall or not. This is very helpful in evaluating the arteriosclerosis and hemodynamic disease-related vascular lesion properties such as the blood flow, velocity, pressure, viscosity, and peripheral resistance.

In conclusion, blood vessel quantification using the linear array PAT is proposed with the compensation of the optical fluence from MC light transport. The co-registered PA and US images of an artificial vessel is first obtained to verify the numerical simulation hypothesis and the US/PA images of human peripheral vessels in the forearm are achieved afterward, demonstrating the satisfactory image quality realized with this approach. The US imaging and the fluence compensated PA imaging modalities can not only quantify the location, thickness, or inner diameter, but also differentiate the internal region of interest of the blood vessel from background tissue. It is of great value for the clinical architectural analysis of blood vessels. An MC model that matches the complex

biological tissue structure will be further investigated to achieve more accurate optical fluence compensation. Future studies using this quantitative method will be carried out to evaluate the blood oxygen metabolism and blood flowing in real time.

References

1. C. G. Hoelen, F. F. de Mul, R. Pongers, and A. Dekker, Opt. Lett. **23**, 648 (1998).
2. T. I. Chiu, T. C. Hsiao, S. B. Luo, W. T. Tien, Y. Y. Cheng, and M. L. Li, IEEE Sens. J. **58**, 1772 (2011).
3. L. V. Wang and J. Yao, Nat. Methods **13**, 627 (2016).
4. J. Xia, J. Yao, and L. V. Wang, Prog. Electromagn. Res. **147**, 1 (2014).
5. R. A. Kruger, R. B. Lam, D. R. Reineck, S. P. D. Rio, and R. P. Doyle, Med. Phys. **37**, 6096 (2010).
6. Z. Wu, M. Sun, Q. Wang, T. Liu, N. Feng, J. Liu, and Y. Shen, Chin. Opt. Lett. **12**, 101102 (2014).
7. M. Sivaramakrishnan, K. Maslov, H. F. Zhang, G. Stoica, and L. V. Wang, Phys. Med. Biol. **52**, 1349 (2007).
8. Y. Wang, J. Yuan, S. Du, X. Liu, G. Xu, and X. Wang, Chin. Opt. Lett. **13**, 061001 (2015).
9. Y. Liu, Y. Su, J. Yao, and R. K. Wang, J. X-ray Sci. Technol. **13**, 129 (2005).
10. H. F. Zhang, K. Maslov, G. Stoica, and L. V. Wang, Nat. Biotechnol. **24**, 848 (2006).
11. X. Lin, N. Feng, Y. Qu, D. Chen, Y. Shen, and M. Sun, Chin. Opt. Lett. **15**, 101102 (2017).
12. C. M. Anderson, D. Saloner, R. E. Lee, V. J. Griswold, L. G. Shapeero, J. H. Rapp, S. Nagarkar, X. Pan, and G. A. Gooding, AJNR **13**, 989 (1992).
13. C. Lutzweiler, D. Razansky, L. Ding, V. Ntziachristos, and X. L. Deánben, in *European Conference on Biomedical Optics* 99 (2015).
14. L. Ding, X. L. Dean-Ben, and D. Razansky, IEEE Trans. Med. Imaging **35**, 1883 (2016).
15. M. Sun, N. Feng, Y. Shen, X. Shen, L. Ma, J. Li, and Z. Wu, Opt. Express **19**, 14801 (2011).
16. T. Liu, M. Sun, N. Feng, M. Wang, D. Chen, and Y. Shen, Chin. Opt. Lett. **14**, 091701 (2016).
17. Y. Gao, Y. Deng, X. Tong, H. Wang, Z. Deng, X. Yang, Y. Liu, H. Gong, and Q. Luo, Chin. Opt. Lett. **10**, 061101 (2012).
18. R. G. M. Kolkman, J. H. G. M. Klaessens, E. Hondebrink, J. C. W. Hopman, W. Steenbergen, T. G. V. Leeuwen, J. M. Thijssen, and F. F. M. D. Mul, Proc. SPIE **4960**, 1 (2003).
19. Y. Xu, L. V. Wang, G. Ambartsoumian, and P. Kuchment, Med. Phys. **31**, 724 (2004).
20. S. Bu, Z. Liu, T. Shiina, K. Kondo, M. Yamakawa, K. Fukutani, Y. Someda, and Y. Asao, IEEE Trans. Biomed. Eng. **59**, 1354 (2012).
21. L. Wang, S. L. Jacques, and L. Zheng, Comput. Methods Programs Biomed. **47**, 131 (1995).
22. I. Patrikeev, Y. Y. Petrov, I. Y. Petrova, D. S. Prough, and R. O. Esenaliev, Appl. Opt. **46**, 4820 (2007).
23. S. L. Jacques, Photoacoustics **2**, 137 (2014).
24. R. J. Zemp, Appl. Opt. **49**, 3566 (2010).
25. P. Shao, B. Cox, and R. J. Zemp, Appl. Opt. **50**, 3145 (2011).
26. R. G. Kolkman, J. H. Klaessen, E. Hondebrink, J. C. Hopman, F. F. de Mul, W. Steenbergen, J. M. Thijssen, and T. G. van Leeuwen, Phys. Med. Biol. **49**, 4745 (2004).
27. Y. Liu, H. Jiang, and Z. Yuan, Med. Phys. **43**, 3987 (2016).
28. M. Keijzer, S. L. Jacques, S. A. Prahl, and A. J. Welch, Lasers Surg. Med. **9**, 148 (1989).